THE PHYSICAL BASIS OF THE EXPLOSION SOURCE AND GENERATION OF REGIONAL SEISMIC PHASES

Jeffry L. Stevens, G. Eli Baker, and Heming Xu

Science Applications International Corporation

Sponsored by Air Force Research Laboratory

Contract No. FA8718-04-C-0025

ABSTRACT

A longstanding nuclear monitoring problem is prediction of regional S phases, particularly Lg. Observed Lg is generally larger than predicted from a point source in a plane-layered earth model, particularly in high-velocity source regions. Direct generation of shear waves by a realistic explosion source is a likely explanation of the Lg amplitudes, although other explanations such as redirection of pS or scattering of Rg into Lg have been proposed, and to date it has not been possible to conclusively and quantitatively resolve the mechanisms responsible. We analyze several distinct sets of nuclear explosion records, complemented by nonlinear source and near field scattering calculations, which are coupled to regional waveform calculations, to quantify the effect of separate mechanisms.

We use local records obtained under this contract by the Institute for the Dynamics of the Geospheres (IDG) for 15 Degelen and Balapan explosions to investigate the effect of source depth and location within the Semipalatinsk Test Site (STS) on local generation of Sg and Rg relative to P. The local Sg/Pg ratios span a broad range and correlate well with regional S/P amplitudes recorded at the Borovoye auxiliary seismic station BRVK, at 650 km, suggesting that the local Sg may be the major contributor to regional S. IDG has also delivered parametric information, including depths and yields for nearly all of these events, and depths, yields, and near field waveform parameters (peak velocity, rise time, positive pulse width, and arrival time) for 19 STS nuclear explosions from the 1960s and 1970s.

We also have extended previous work on Nevada Test Site (NTS) and Kazakh depth of burial experiments. Specifically, we extend a comparison of vertical component P and Lg spectra of co-located overburied and normally buried explosions at NTS to 3-components and to Lg coda. Interpretation of a null previously observed in vertical component Lg spectral ratios is complicated by a corresponding peak in the Lg spectra of the overburied events. The null, however is clearly observed in the raw vertical component Lg spectra of normally buried events. It is somewhat inconsistent in the horizontal component Lg, and it is not present at all in the Lg coda. Rg scattered to Lg in modal scattering calculations for an NTS structure, however, is more prominent in the Lg coda time window (due to excitation of slower modes) than in the Lg. Wave number synthetics for spherical and CLVD point explosions and the modal scattering calculations also indicate that directly generated S and trapped pS in an NTS structure have similar nulls and contribute more to the Lg spectra than does scattered compensated linear vector dipole (CLVD) Rg. We are currently analyzing results of nonlinear source calculations for a normally buried and overburied explosion.

We also extend analysis of Kazakh depth-of-burial explosion data to 3-components. We find distinct Sg, separate from Rg, and extending to higher frequencies than Rg, on all 3-components of the local records of all three events. The local Sg is most prominent on the records of the two shallower events. Rg is still the dominant phase in near regional (85 km) records at KUR, where it is again preceded by a distinct S phase. These observations are consistent with S generated by the source, trapped pS, and possibly S* being major contributors to Lg.

OBJECTIVE

The objective of this project is to determine the source physics and corresponding generation and evolution of local and regional seismic waves from nuclear explosions. This is a joint project between the Science applications International Corporation (SAIC) and the Institute for the Dynamics of the Geospheres (IDG) in Moscow, Russia.

RESEARCH ACCOMPLISHED

Introduction

Lg is important to explosion yield estimation and earthquake/explosion discrimination, but the source of explosion generated Lg is still an area of active investigation. A spherical explosion in a whole space generates no shear waves. Thus, in the earth, shear waves from explosions must be generated by non-spherical components of the source, due to some asymmetry of the source or source conditions, or tectonic strain release, or by conversion of P and/or Rg waves to S, particularly though surface Rg scattering and surface P-to-S conversion including generation of S* (the strongly depth dependent nongeometric phase generated by conversion of the curved P wavefront).

In this project, we have been trying to constrain the source of Lg and other regional phases by examination of unique data sets from historical Soviet nuclear explosions, combined with theoretical analysis and numerical modeling. We examine local and regional data from these explosions to directly observe the generation, propagation and attenuation of S phases and the Rg phase. Most of the proposed mechanisms for Lg generation have a significant dependence on depth and/or scaled depth. We have excellent constraints on the yield and depths of the Soviet explosions and so can examine this dependence directly. In addition to regional phase generation, we also use new Soviet data from explosions detonated close to earlier explosions to determine the effect of proximity to an earlier event on coupling efficiency.

New Local Semipalatinsk Data: Description and Analyses

The Russian Institute for the Dynamics of the Geospheres (IDG) has provided two types of data. First is parametric data, depth, yield, peak velocities, and rise times for 25 Semipalatinsk nuclear explosions (Table 1). Event selection focused on sets of adjacent events to enable analysis of the effect of previous nearby events on the waveforms. IDG also provided 275 unique seismograms for 17 nuclear explosions with time series extending past the Rg arrival (Table 2). We are comparing local P, S, and Rg amplitudes with depth, yield, scaled depth, and with corresponding measurements at regional distance (BRVK, 650 km).

The near field data from some events in close proximity to earlier events were indistinguishable from the earlier events; however, a few events that were detonated close to an earlier event have distinctly different near field data. In Table 1, those events that were both close to an earlier event and which had significantly different near field peak velocity measurements than the earlier event are marked.

Figure 1 shows a map of part of the Degelen test site with 5 events marked (listed by number in Table 1). Peak velocity vs. scaled range measurements (Figure 1, right side) show that events 13 and 14 have significantly lower peak particle velocities than the earlier event that they were very close to: event 11. Event 15 was also close to event 12, but the effect on particle velocity is less clear than for events 13 and 14. The other two events marked in Table 1 were also close to an earlier event and had significantly reduced peak velocities.

Despite the significant effect on peak velocities for some events in the near field, there is no apparent effect on m_b. The events with reduced near field peak velocity fall right into the population of other explosions in a plot of m_b vs. yield (Figure 2) and are quite close to the magnitude/yield curve for this region ($m_b = 0.75\log Y + 4.45$, where Y is yield in kilotons; Murphy, 1995).

Table 1. Near field tabular data collected by IDG.

Date	Yield (kt)	Depth (m)	m_b	Event No.	Near Earlier Event	Lat	Lon
61/10/11	1.16	141	[K]4.78			49.772	77.995
62/02/02	16.9	265	[K]5.63			49.778	78.002
64/03/15	23.6	245	[A]5.56			49.808	78.102
64/05/16	23.7	266	[A]5.55	11		49.775	77.988
64/06/06	1.05	75	[K]4.42			49.809	78.093
64/11/16	23	203	[A]5.64			49.809	78.133
65/02/04	17	262	[A]5.10		X	[2]49.773	[2]77.991
65/07/29	1.0	126	[I]4.5			[2]49.773	[2]77.991
65/06/17	12	178	[A]5.24			49.828	78.067
65/09/17	10	148	[A]5.22			49.812	78.147
65/10/08	15	204	[A]5.47	12		49.826	78.111
65/11/21	29	303	[A]5.61			49.819	78.064
65/12/24	6	228	[A]4.94	13	X	49.805	78.107
66/02/13	109-125	343	[A]6.26			49.809	78.121
67/12/08	12.5	166	[A]5.31			49.817	78.164
68/09/29	75	358	[A]5.8			49.812	78.122
73/02/16	25	225	[A]5.48	14	X	49.816	78.116
79/05/31	8.5	183	[A]5.27		X	49.830	78.087
80/06/25	0.3	152	[K]3.70	15		49.826	78.099

m_b from AWE, Khalturin et al (2001) or ISC

Table 2. Local/near regional data collected by IDG that contain Rg arrivals. SD stands for scaled depth, column 6 lists the number of distinct seismograms for each component (there are multiple recordings at many distances—we count these only once). The last column lists location within Semipalatinsk, D for Degelen or B for Balapan.

Date	Time	Yield	Depth	SD	Data t/r/z	Range (km)	m_b	Lat	Lon	Loc
[1]71/12/15	07:52:59	1.3-1.5	146	1.07	3/9/9	7-77	[A]4.68	50.031	77.972	D
85/06/30	02:39:05	100	527	0.93	0/6/5	49-88	[A]5.92	49.857	78.659	B
85/07/20	00:53:16	76	466	0.90	0/8/7	56-86	[A]5.89	49.943	78.783	B
[1]87/05/06	04:02:08	18	174	0.54	0/9/9	13-83	[I]5.6	49.777	77.984	D
[1]87/07/17	01:17:09	78	267	0.51	1/7/6	15-84	[I]5.8	49.769	78.035	D
[1]87/10/16	06:06:07	1.1	82	0.65	0/8/8	19-76	[I]4.6	49.802	78.14	D
87/12/13	03:21:07	130	530	0.86	0/5/5	57-60	[A]6.06	49.957	78.792	B
[1]88/04/22	09:30:09	2	---	---	0/3/3	57-81	[I] 4.9	49.824	78.102	D
88/05/04	00:57:06	134	530	0.85	0/6/4	53-84	[A]6.09	49.931	78.741	B
88/06/14	02:27:09	5	271	1.30	0/7/6	67-89	[A]4.8	50.034	78.964	B
88/09/14	04:00:00	140	651	1.03	3/7/7	60-94	[A]6.03	49.879	78.823	B
88/11/12	03:30:06	17	---	---	5/6/7	68-88	[A]5.24	50.048	78.96	B
[1]88/11/23	03:57:09	19	204	0.63	6/9/9	14-83	[I]5.4	49.765	78.029	D
88/12/17	04:18:09	84	642	1.20	6/6/6	67-98	[A]5.83	49.879	78.924	B
89/01/22	03:57:09	108	580	1.00	6/9/9	58-88	[A]6.10	49.934	78.815	B
89/02/12	04:15:09	74	572	1.12	4/7/9	51-85	[A]5.86	49.911	78.704	B
[1]89/10/04	11:29:57	1.8	94	0.63	5/8/7	16-85	[I]4.6	49.751	78.005	D

[1] More data from previously reported event, with longer time series that include Rg.
[A] and [I] indicate m_b from the United Kingdom's Atomic Weapons Establishment (AWE) and the International Seismological Centre (ISC), respectively.
Locations from Geoscience Australia's database (http://www.ga.gov.au/oracle/nukexp_form.jsp)

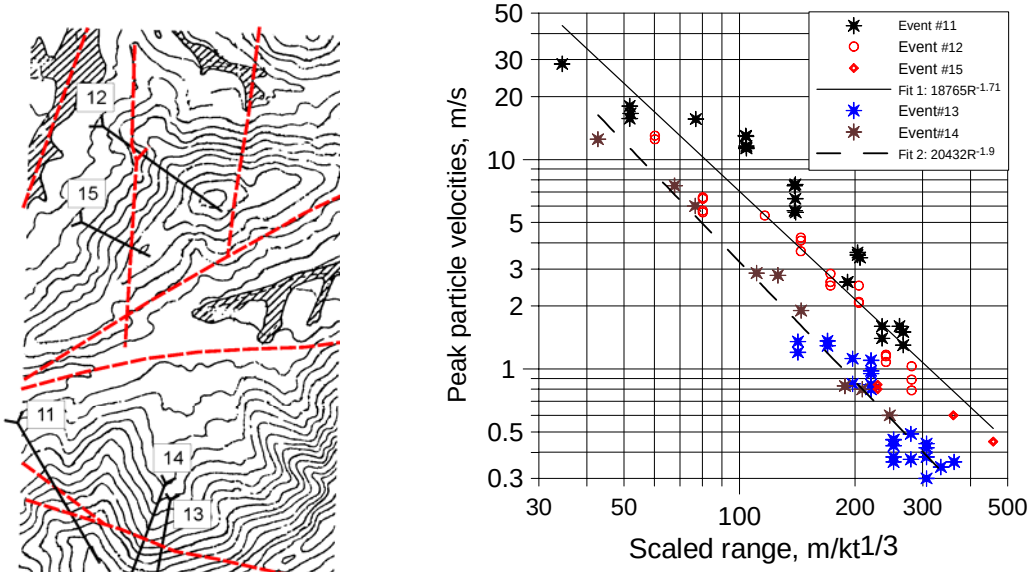

Figure 1. Location of five Degelen explosions (left) and peak particle velocity vs. scaled range (right). Lines on the map show tunnels from the tunnel entrance to the shot location. Number is by the entrance point. Red lines are fault locations. Peak velocities are lower than is typical for some events located near previous events.

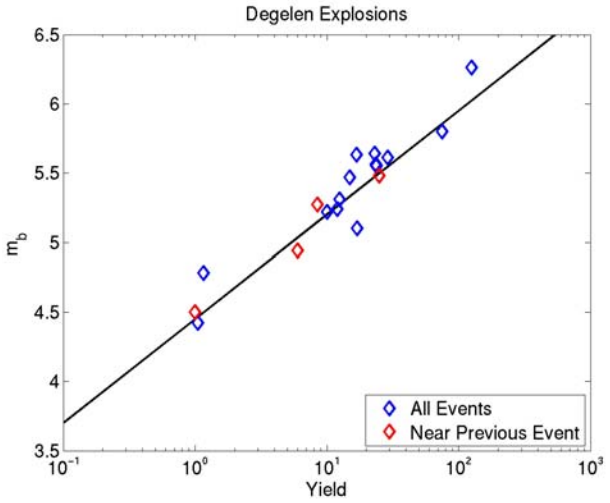

Figure 2. m_b vs. yield for the events in Table 1. Red triangles mark the four events marked in Table 1 as close to another event and having reduced near field peak velocities. The solid line is the nominal m_b/yield curve for this region from Murphy (1995). The effect of previous events on local peak velocities (Figure 1) is not observed in m_b.

Figure 3 shows local records of each of the Balapan explosions recorded at approximately 80 km (left) vs. the corresponding record from BRVK, at approximately 685 km. Figure 4 shows the same for the Degelen explosions. Both the local and regional records are normalized by the P-wave amplitudes. The Degelen records have much larger Sn and Lg amplitudes relative to P, which may be explained by the relative source spectra of S and P. That is, the Balapan explosions are mostly at yields and depths where the corner frequencies of the predicted P and S source spectra fall toward the left edge of the 0.5 to 2 Hz frequency band. The S spectral corners of the smaller Degelen explosions are more likely to be to the right of the frequency band we are examining. Figure 5 shows the predicted P and S-wave source spectra in granite (Mueller and Murphy, 1971; Murphy 2006) for the 74 and 5 kt Balapan explosions. The predicted source spectra are consistent not only with larger regional S/P for Degelen than for Balapan events, but also with the more distinct Sn and larger Lg from the smallest Balapan explosion (Figure 3,

bottom trace) and smaller Sn and Lg for the largest Degelen explosion (Figure 4, top trace). It is also consistent with the observations and conclusions of Fisk et al. (2005) regarding regional S/P from Lop Nor explosions. A second important observation made from these new data is that local Sg/Pg ratios are positively correlated with regional S/P ratios.

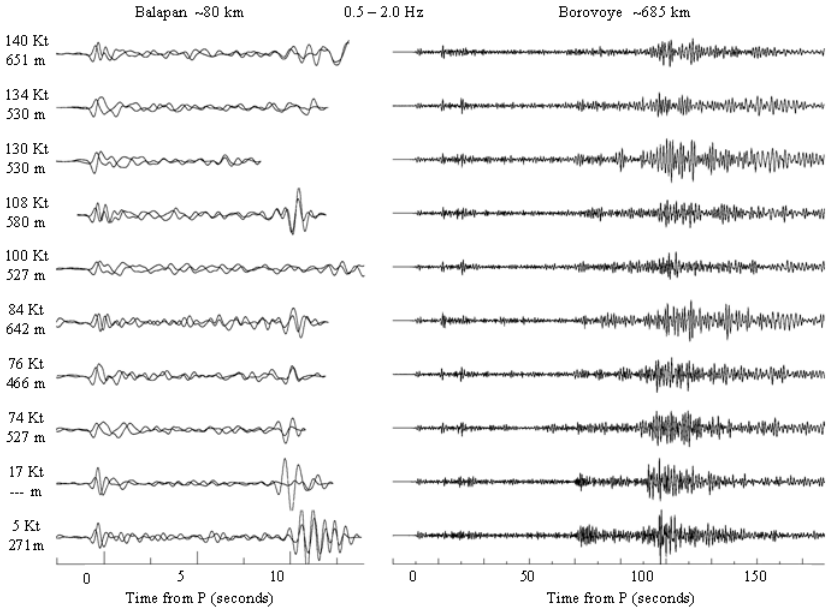

Figure 3. Overlain vertical and Hilbert transformed radial records of Balapan explosions (the closest record to 80 km distance for each event is plotted). To highlight S the large Rg is not plotted (left). Vertical records of the same events at BRVK, at 680 to 690 km, are plotted on the right. Both local and regional records are normalized by their P-wave amplitudes. Yields and depths are noted to the left of the traces. Sn is not prominent, and Lg is relatively small except for the smallest events.

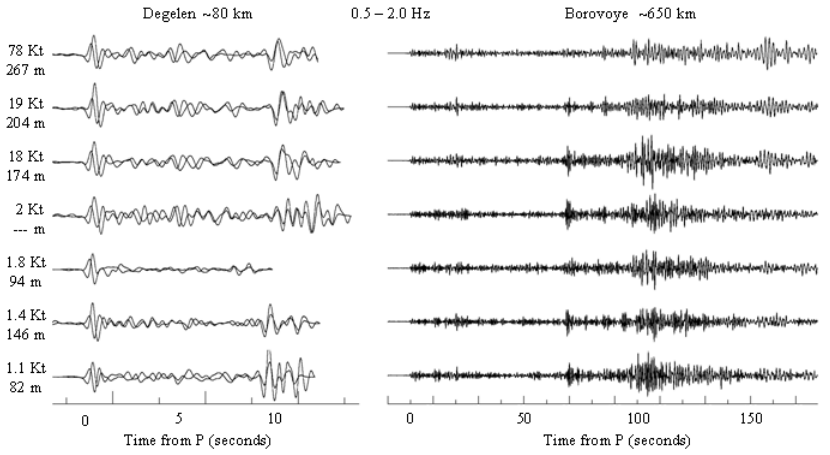

Figure 4. Same as Figure 2, but for Degelen explosions. Sn and Lg are prominent and large, except for the largest events, which appear more similar to the Balapan explosion records. The difference in S/P ratios may be accounted for by P and S source scaling (Figure 5).

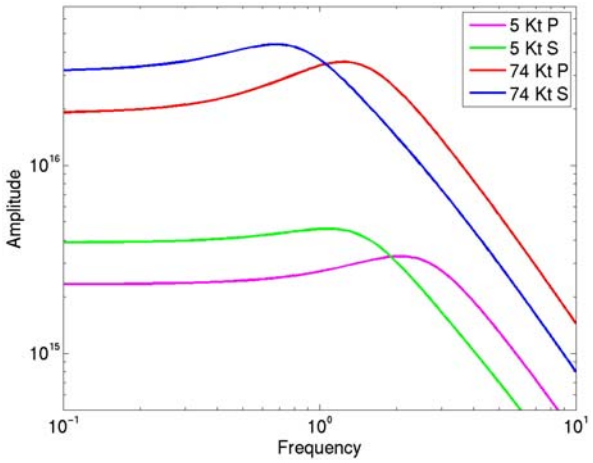

Figure 5. P and S source spectra for the 74 Kt, 572 m depth (2/12/89) and the 5 Kt, 271 m depth (6/14/88) Semipalatinsk explosions. The P spectrum is a Mueller Murphy granite source; the S spectrum is the Mueller Murphy source with the P wave speed replaced by the S wave speed, which shifts the spectrum to lower frequency for the S phase. This causes the S waves to appear to grow relative to P with decreasing explosion yield.

New Analysis of NTS Records

Patton and Taylor (1995) attribute a consistent spectral null at 0.55 Hz in the ratio of Lg spectra from normally buried to overburied explosions to CLVD generated Rg scattering to Lg. We extend analysis of the data used by Patton and Taylor to 3-components and to coda spectra, and use nonlinear source calculations, modal calculations, and wavenumber integration to model the results. Patton and Taylor (1995) normalized the vertical component Pg and Lg spectra of three normally buried explosions by those of two nearby overburied explosions to isolate the effects of spall. We do not use spectral ratios, because a spectral peak at 0.55 Hz in the overburied events' spectra causes a corresponding null in spectral ratios, which makes interpretation ambiguous. Table 3 lists the distances from the normally buried events to each of the overburied events, yields based on m_b(Lg), depths, scaled depths, and which components were available at each of the four Lawrence Livermore National Laboratory (LLNL) stations used for the five events used by Patton and Taylor.

Figure 6 shows the network averaged spectra for Pg, Lg (3.6 to 3.0 km/s), and Lg coda (3.0 to 2.0 km/s), for all three components. There is a clear spectral null in the vertical component Lg, and less distinct but similar nulls in Baseball and Caprock's, but not Glencoe's radial Lg. There is no clear corresponding null in the tangential Lg spectra, although Baseball has a null at slightly higher frequency. There are no corresponding nulls in any component of the Lg coda for any of the events.

Table 3. Metadata and availability of 3-component data from NTS events used in Taylor and Patton (1995) to investigate the effects of spall. The fifth column, SD, indicates scaled depth.

	Dist[1] (km)	Dist[2] (km)	Y=y(m_b)	Depth (m)	SD	ELK 412 km	MNV 238 km	LAC 301 km	KNB 287 km
Caprock	0.34	1.36	264	600	0.77	-	T,R,Z	T,R,Z	N,Z
Baseball	2.14	0.45	117	564	0.94	T,R,Z	T,R,Z	T,R,Z	T,R,Z
Glencoe	2.97	2.06	101	610	1.07	N,Z	T,R,Z	T,R,Z	E,Z[3]
Techado	-	1.70	2.89	533	3.07	T,R,Z	T,R,Z	T,R,Z	Z
Borrego	1.70	-	0.868	564	4.85	T,R,Z	T,R,Z	T,R,Z	T,R,Z

[1] Distance from Techado
[2] Distance from Borrego
[3] East component exists but is extremely poor quality

Modal simulations for an NTS structure indicate that, even for instantaneous scattering of all Rg to higher modes, the scattered Rg contributes more to the Lg coda time window than it does to Lg. This suggests that if the observed null is due to scattered CLVD Rg, the null should also be prominent in the Lg coda. The absence of the null in the coda spectra raises the question of which other sources of Lg could account for the observed null. Figure 7 shows the contributions to Lg from trapped pS, direct S from a CLVD source, scattered explosion Rg, and scattered CLVD Rg, all calculated for an NTS structure. The spherical explosion source is at 500 m depth, and the CLVD is half the moment of the explosion and is at 300 m depth. The scattered Rg contributions assume instantaneous scattering of all Rg energy into higher modes, with the distribution determined by a vertical point force (Stevens et al., 2005).

Time series are on the left and spectra on the right. Each of the contributions has a null in the same frequency band, but the amplitude of CLVD Rg contribution is approximately an order of magnitude smaller than that of other sources of Lg.

Actual nuclear explosion sources have some spatial and temporal distribution, which could affect their spectral shape. Figure 8 shows the regions of permanent nonlinear deformation and cracking from 2D nonlinear calculations of the Baseball and Techado sources. It also shows the Lg spectra of the Baseball (blue) and Techado (red) calculations compared with the sum of a spherical point explosion and a CLVD of half the explosion's size (black, dashed). The Lg of all three share a 0.55 Hz null. The common Lg spectral nulls demonstrate that the trapped pS and direct S from the nonspherical parts of the source are sufficient to explain the observed spectral nulls, and that the nulls persist for a more realistic distributed source. This analysis demonstrates that Lg spectral nulls can be generated by direct S and pS in an NTS structure, but, because increased scattering in the coda could obscure nulls there, the lack of nulls in Lg coda alone is insufficient to rule out other possible mechanisms.

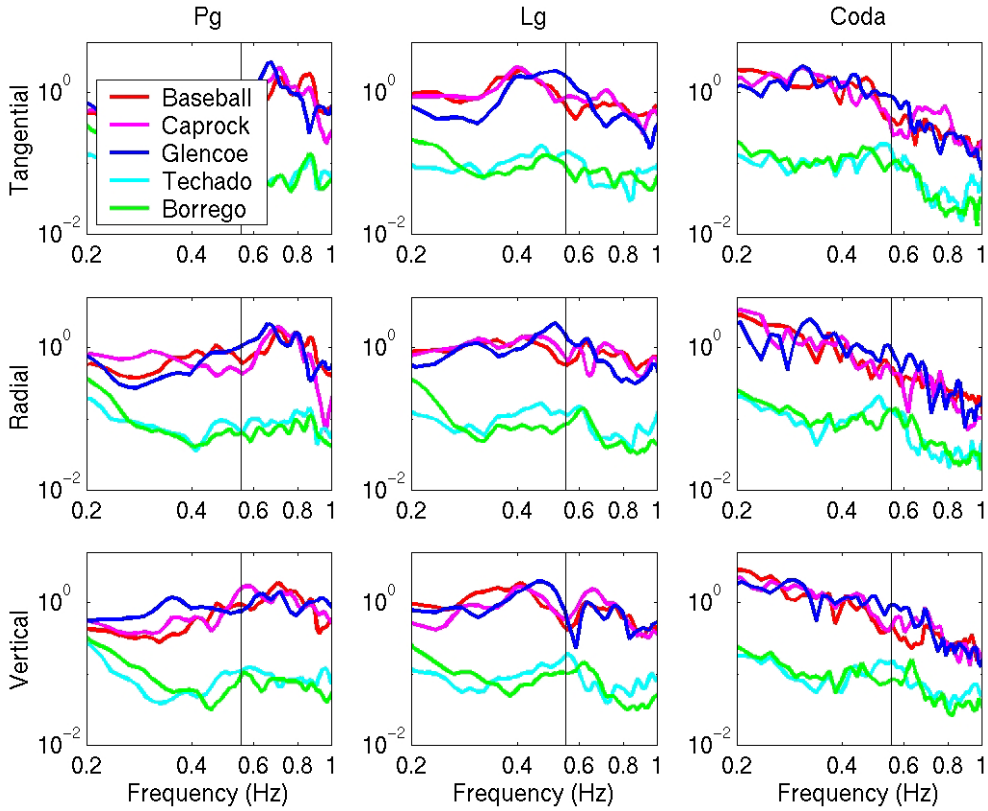

Figure 6. Network average Pg, Lg, and Lg coda spectra for all 3-components for Baseball (red), Caprock (purple), Glencoe (blue), Techado (aquamarine), and Borrego (green). The 0.55 Hz, black, vertical line shows the vertical component Lg spectral null position for the normally buried events. The null is not observed in the Lg coda, or as consistently in other components of Lg.

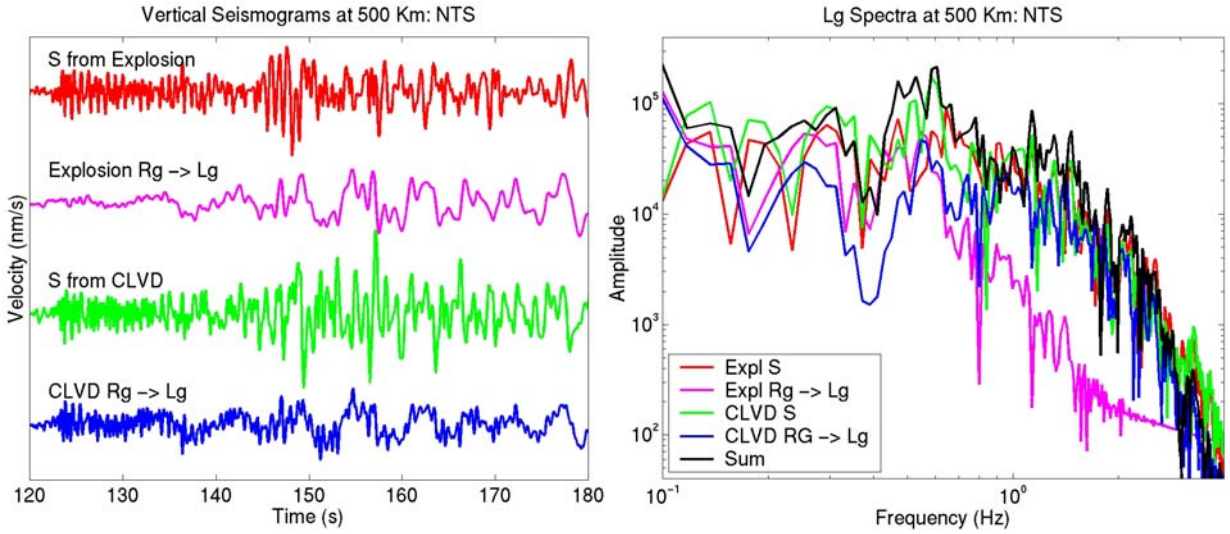

Figure 7. Contributions to the time series within the Lg window (left) and their spectra (right). Trapped pS (red), spherical explosion Rg to Lg scattering (maroon, upper bound), direct S from a CLVD (green), and CLVD Rg to Lg scattering (blue, upper bound) share a common spectral null, but the scattered CLVD Rg contributes less than the others. The black spectral curve is the sum of all the contributions.

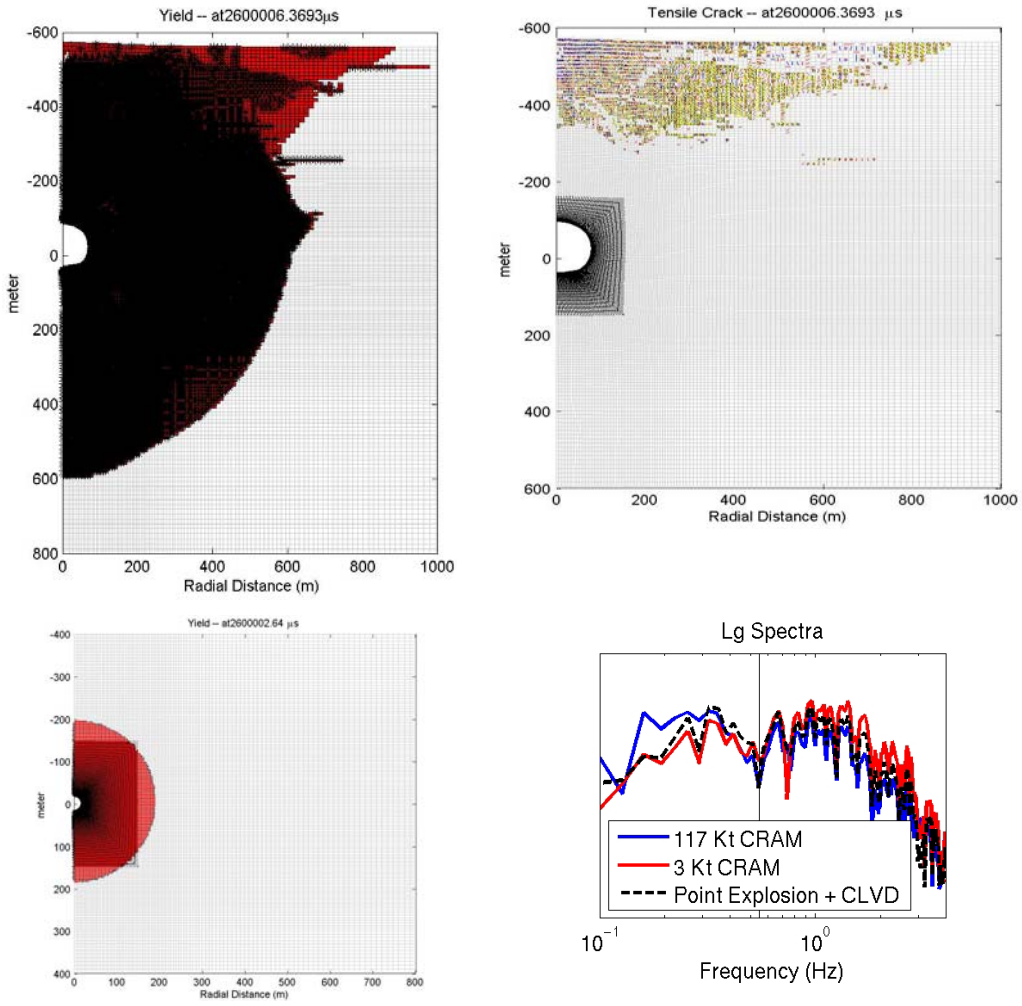

Figure 8. Permanent nonlinear deformation (left column) produced by 2D Lagrangian finite-difference simulations of the sources of Baseball (top) and Techado (bottom). The simulation for Techado produces a nearly spherical area of permanent deformation and no cracks. Cracks predicted by the Baseball simulation are shown in the upper right. Lg from these nonlinear source calculations for the Baseball (blue), Techado (red), and the sum of an explosion and a CVLD of half the explosion's size (black, dashed). The vertical black line indicates 0.55 Hz.

New Analysis of Kazakh Depth of Burial Experiments

Three 25-ton explosions were detonated at Balapan to investigate the effect of burial depth (Glenn and Myers, 1997). Myers et al. (1999) attribute spectral differences between regional P/S amplitude ratios to depth dependent differences in Rg, which is assumed to scatter to S. Patton et al. (2005) suggest that m_b(Lg) differences they observe at 415 km are due to differences in the amount of Rg available from each explosion for scattering to Lg near the source. The observed regional phase amplitudes may also be explained by differences in S directly generated at the source, due to structure and lack of containment for the shallow event. Direct generation of S from the explosions that reproduces the observed regional S/P ratios would predict Sg distinct from Rg near the source, and local S/P ratios consistent with regional S/P. To evaluate this prediction, we extend the previous work by examining 3-component local records to identify local Sg. We also examine an additional record at 85 km to investigate the persistence of Rg.

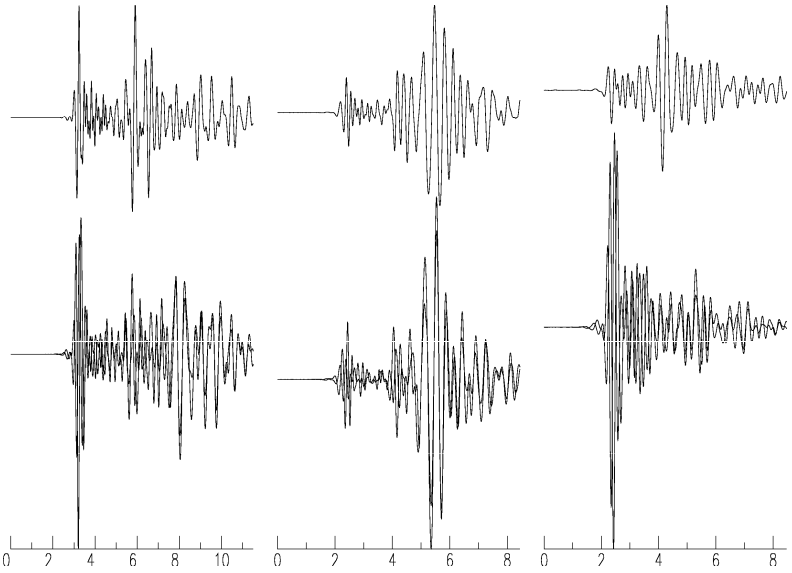

Figure 9. Tangential (upper) and overlain vertical and Hilbert transformed radial (lower) records of the 50, 300, and 550 m depth events (from left to right), filtered from 2 to 5 Hz. All three records in each set share the same scale. Records are at 17.3, 12.7, and 12.7 km respectively, and are plotted from origin time to 1.5 km/s group velocity. In each, a distinct Sg precedes the Rg (off azimuth for the 300 m depth event). Sg is more commonly observed and larger for the two shallowest explosions. Rg is smallest for the deepest event.

Figure 9 shows one 3-component set of local records for each event, filtered from 2 to 5 Hz, at 17.3, 12.7, and 12.7 km distance respectively for the 50, 300, and 550 m depth events. All records for each 3-component set are plotted on the same scale. Sg is distinguishable on all three components of records from all three events. Record sections (not shown due to space limitations) show that these Sg observations are not unique to just the records shown, and that Sg is generally most prominent on the records of the two shallower events. The Sg persists to frequencies greater than those of Rg, suggesting that they are not merely scattered from Rg.

Differences in source parameters besides depth, and the multiplicity of mechanisms that have some depth dependence complicate interpretation of the observed differences in S-wave generation between explosions. The shallowest explosion, which cratered, took place in “a weak shale” (Glenn and Myers, 1997), while the other two explosions were in granite. For the shallowest explosion, S*, the cratering, and more generally the asphericity of the yielding region, which generates shear waves directly, should all contribute to generate more shear waves than come from the deeper explosions. Although the two deeper explosions are very overburied, so we might not normally expect much asphericity, acceleration records show evidence of spall at depths associated with weak zones in both cases (Patton et al., 2005). Also, the P-wave velocity of the weak shale is less than the mantle shear wave velocity, and so the surface pS converted phase should be trapped and contribute significantly to Lg. Trapping of pS is less certain for the deeper sources, where source P-wave velocities are near the mantle S-wave velocity.

The importance of scattered Rg as a source of S depends on the rate of near source Rg scattering. Modal scattering upper bound calculations for a Degelen structure, similar to those in Figure 6, indicate that even if all CLVD Rg is scattered instantaneously at the source, it contributes less to Lg above 0.5 Hz than does direct S from the same CLVD. Ongoing work includes similar calculations for the structure local to these events at the event depths with more realistic rates of Rg scattering. Myers et al. (1999) observe that Rg is rapidly attenuated at < 20 km. We however observe that for all three explosions, below 2 Hz, Rg is still the dominant phase at KUR, 85 km distance (Figure 10). The Rg, arriving at approximately 30 s, is so dominant at 0.5 to 1 Hz that it is almost the only phase visible. At 1–2 Hz it is still larger than P and as large as the S phase, which arrives at approximately 20 s. This observation provides a limit on the energy available for near source scattering of Rg to regional S.

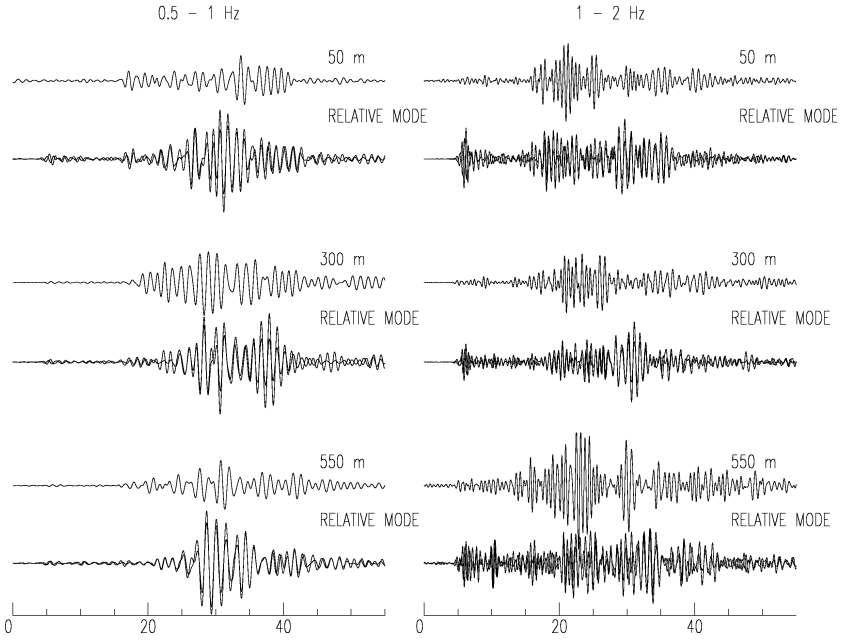

Figure 10. Shown here are 3-component seismograms for the 50 (upper set), 300 (middle), and 550 (lower) m depth of burial explosions at 85 km distance, at station KUR, from 0.5–1 Hz (left) and 1–2 Hz (right). Sg (at ~20 s) is distinct from the large Rg (~30 s) is apparent on the tangential component (upper traces of sets) and the overlain vertical and the Hilbert transformed radial seismograms (lower traces).

CONCLUSION AND RECOMMENDATIONS

We have collected extensive new data sets, including depths and yields, from the Semipalatinsk test site. These have proven useful in demonstrating decreased local peak velocities for some events located near previous explosions, although there is no apparent corresponding effect on m_b. Comparison of the new local records with regional data indicates that local Sg/Pg amplitudes correlate positively with regional S/P. That and the existence of distinct Sg, separate from Rg, for all events suggest that the source of Sg could be the same as that of Sn and Lg. Decreased S/P ratios for larger events can be explained by yield and depth dependent differences in source spectra.

Analysis of data from adjacent normally and overburied NTS events, and of the Kazakh depth of burial experiments, both previously interpreted as supporting Rg scattering to Lg, indicates that direct generation of S at the sources could also explain the observations. Numerical simulations, including modal scattering calculations, indicate that for the NTS events, both pS and direct S from a CLVD should contribute more to Lg than does scattered Rg from a CLVD. Nonlinear source calculations demonstrate that spectral nulls associated with pS and direct S from a CLVD are preserved for a more realistic distributed source. For the Kazakh depth of burial explosions, similar calculations indicate the same conclusion for the direct CLVD S, but further simulations at the depth of each explosion should be performed. For these calculations, Rg decay from local records and KUR should be employed to constrain the upper bound on Rg energy available for scattering to Lg.

REFERENCES

Fisk, M., T. Lay, and S. Taylor (2005). Modeling and empirical research on energy partitioning of regional seismic phases used for explosion monitoring, in *Proceedings of the 27th Seismic Research Review: Ground-Based Nuclear Explosion Monitoring Technologies*, LA-UR-05-6407, Vol. 1, pp. 539–549.

Glenn., L. and S. Myers (1997). Depth of Burial Experiments at Balapan, Univ. of CA, LLNL Report.

Khalturin, V., T. Rautian, and P. Richards (2001). A study of small magnitude seismic events during 1961-1989 near and on the Semipalatinsk Test Site, Kazakhstan, *Pure and Applied Geophysics* 158: 143–171.

Myers, S. C., W. Walter, K. Mayeda, and L. Glenn (1999). Observations in support of Rg scattering as a source for explosion S-waves: regional and local recordings of the 1997 Kazakhstan depth of burial experiment, *Bull. Seism. Soc. Am*. 89: 544–549.

Mueller, C. and J. Murphy (1971). Seismic characteristics of underground nuclear detonations Part I: seismic spectrum scaling, *Bull. Seis. Soc. Am.* 61: 1675–1692.

Murphy, J. R. (1995). Types of seismic events and their source descriptions, in monitoring a comprehensive test ban treaty, ed. E. Husebye and A. Dainty, pp. 225–245, Kluwer Academic Publishers, Boston.

Murphy, J. R. (2006). Source scaling analyses of frequency dependent energy partition for regional P and S phases from explosion sources, *Seis. Res. Lett.* **77**: March/April, p. 196.

Patton H. and S. Taylor (1995). Analysis of Lg spectral ratios from NTS explosions: implications for the source mechanisms of spall and the generation of Lg waves, *Bull. Seism. Soc. Am.* 85: 220–236.

Patton, H., J. Bonner, and I. Gupta (2005). Rg excitation by underground explosions: insights from source modeling the 1997 Kazakhstan depth-of-burial experiment, *Geophys. J. Int*. 163: 1006–1024.

Stevens, Jeffry L., G. Eli Baker, Heming Xu, and Theron J. Bennett (2005). The physical basis of the explosion source and generation of regional phases, in *Proceedings of the 27th Seismic Research Review: Ground-Based Nuclear Explosion Monitoring Technologies*, LA-UR-05-6407, Vol. 1, pp. 663–672.